Optical Pumping*

Kazem Ayat†
Physics Department, University Of California: Berkeley
(Dated: May 3, 2023)

Abstract

This lab report aimed to investigate and calculate various parameters related to Rubidium atoms, including the ambient magnetic field, and nuclear spin values. Through data analysis and calculations, the ambient field for Rb87 was found to be (-0.4282 ± 0.004)G and for Rb85 to be (-0.4352 ± 0.006)G, which matches well with the accepted range for the value of the earth's magnetic field. The nuclear spin values for Rb85 and Rb87 were determined to be 2.539 ± 0.004 and 1.532 ± 0.006, respectively, which closely resemble the perfect ratios of 5/2 and 3/2. Finally, the optical pumping phenomenon was explained, with Rubidium's electron configuration and our tools. These results demonstrate the success of the experimental measurements and calculations in accurately determining important parameters of Rubidium atoms. Throughout this experiment, we have acquired a wealth of knowledge in several areas of physics, particularly in the field of quantum mechanics. Our observations have allowed us to directly witness the existence and behavior of quantum mechanics in action.

I. INTRODUCTION TO OPTICAL PUMPING

Optical pumping is a phenomenon in physics where atoms are excited from a lower energy state to a higher energy state by shining light of a specific frequency onto a collection of atoms in a magnetic field. The name "optical pumping" comes from the analogy of pumping water into a bucket. In the same way that water can be pumped into a bucket to raise its level, light can be "pumped" into an atom to raise it to a higher energy level. This process causes the electrons in the atoms to absorb the energy of the light and jump to higher energy levels. Once in the higher energy state, the atoms can be used for a variety of applications,As some of it will be covered in this report in depth. Alfred Kastler, who won the Nobel Prize in Physics in 1966 for his work on optical pumping, first used this analogy.

II. THEORY

In this section we will cover the working principles behind performing the Optical pumping experiment!

A. Atomic Structure

We are using Rubidium throughout. It is an alkali-metal atom with atomic number 37. The electron configuration is of the form: [Kr] 5S1. This means that 36 of the 37 bound electrons form a closed inert shell, while the last remaining valence electron occupies the 5s atomic orbital. Naturally, the first excited state of the valance electron is 5P. This excitation happens around 1.6 eV.

So consider all the good old H-atom quantum numbers (n,l,m,s). Principal quantum number (n), Azimuthal quantum number (l), Magnetic quantum number (m), and Spin quantum number for the electron (s)

There is also another quantum number for relevant situations in quantum physics (I-Upper case I): In atomic physics, the nuclear spin quantum number I is a quantum number that characterizes the intrinsic angular momentum of the nucleus of an atom. Just as electrons have an intrinsic spin, protons, and neutrons, which make up the nucleus of an atom, also have intrinsic spin. The nuclear spin quantum number is used to describe the total angular momentum of the nucleus, which depends on the number of protons and neutrons in the nucleus and how they are arranged. The reason we do not consider the nuclear spin quantum number I in the hydrogen atom is that hydrogen has only one proton in its nucleus and no neutrons. Protons have a nuclear spin of 1/2, but since there is only one proton in the hydrogen nucleus, the total nuclear spin is also 1/2. However, since the electron is not affected by the proton's spin in the hydrogen atom, the nuclear spin quantum number I is not relevant to the electron's behavior in the atom. Therefore, we do not need to consider the nuclear spin quantum number when describing the quantum state of the electron in hydrogen.

Hence, now the relevant Quantum numbers for atoms like Rubidium (with Neutron as well) are:

Principal quantum number (n), Azimuthal quantum number (L), Magnetic quantum number (m), Spin quantum number for the electron (S) , and Spin quantum number for the nucleus (I). So, for the 5s ground state,

* From now on we might call optical pumping OPT.
† Also at Physics Department, University Of California:Berkeley

we have L = 0, while for the 5p excited state, we have L = 1. The electron spin is S = $\frac{1}{2}$ for both Rb85 and Rb87, Which is the spin of the single valence electron. But The nuclear spins turn out to be different for the two isotopes: I = 5/2 for Rb-85, and I = 3/2 for Rb-87.

By using this formula we can find the number of states: (2L + 1) × (2S + 1) × (2I + 1) For example, the 5s electronic ground state is actually comprised of 10 states for 85Rb and 8 for 87Rb, respectively. In a similar vein, the 5p electronic excited state consists of a total of 30 states for 85Rb and 24 for 87Rb, respectively. These states represent varying orientations of the azimuthal quantum orbital number, the electron, and nuclear spin.

Now there are corrections to the plain Hamiltonian of the Hydrogen atom. These corrections lead to the splitting of the spectral lines. The first correction is the "Fine structure correction". Fine structure corrections are small corrections to the energy levels of an atom due to relativistic effects and the spin-orbit interaction between the electron's spin and its motion around the nucleus (spin-orbit coupling). The relativistic correction arises because the electron's speed is a significant fraction of the speed of light, while the spin-orbit interaction arises from the magnetic field generated by the moving electron, which interacts with the magnetic field produced by the positively charged nucleus (please refer to fig.2 and fig.1 to see how these splittings happen). Note that $\mathbf{J} = \mathbf{L} + \mathbf{S}$ ($\mathbf{J}$ is called the total angular momentum quantum number in the context of fine structure).

The next level of refinement in setting up the Hamiltonian is referred to as the hyper fine structure, which arises due to the interplay between the electronic angular momentum and the nuclear spin interactions. Note that $\mathbf{F} = \mathbf{I} + \mathbf{J}$. The atom will split up into manifolds of states, each of which has a well-defined total angular momentum quantum number in the context of Hyperfine structure F (please refer to fig.2 and fig.1 to see how these splittings happen).

If an atom undergoes a transition from one energy level to another through the absorption or emission of a photon with a specific frequency. In the presence of an external magnetic field, the energy levels of the atom are split into sub-levels known as Zeeman levels, which have slightly different energies due to the interaction between the magnetic field and the atom's magnetic moment. When the frequency of a photon matches the energy difference between two Zeeman levels, the atom can absorb the photon and transition from the lower to the higher energy level. Conversely, when an atom in a higher energy level spontaneously emits a photon, it can transition to a lower energy level, with the emitted photon carrying away the excess energy. These resonant transitions are important and they play a key role in understanding the behavior of atoms and molecules in the presence of magnetic fields. Our goal in this experiment is to drive and observe the effects of Zeeman transitions in the electronic ground states of rubidium atoms. As visible in fig2 and fig.1 Zeeman transition divides the energy spectrum into even finer subdivisions. Note that all the splittings are due to the intrinsic nature of the atoms, but Zeeman splittings are due to an external conditions (i.e. external magnetic field).

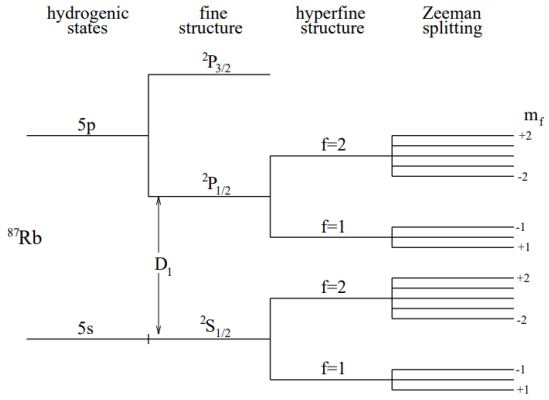

FIG. 1. The fine, hyper-fine, and Zeeman splittings, with the transitions between these levels that are important this experiment for Rb87 [2]

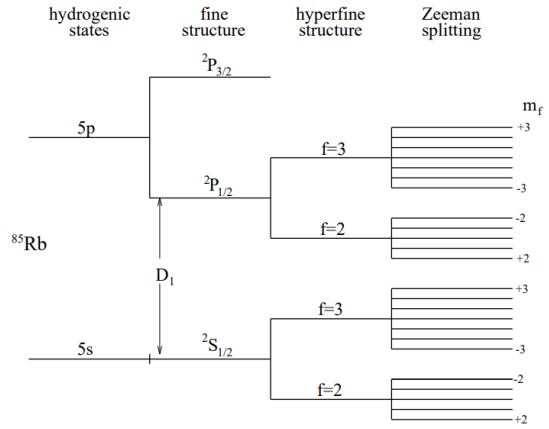

FIG. 2. The fine, hyper-fine, and Zeeman splittings, with the transitions between these levels that are important this experiment for Rb85 [2]

B. Rubidium in a Magnetic Field

Once a Rubidium atom is placed in an external magnetic field (B_{ext}), The Hamiltonian of our Rubidium atom system is (up to Hyper-fine structure):

$$H_{hfs} = -\mu_I.(B_J + B_{\text{ext}}) - \mu_J.B_{\text{ext}}$$

which

$$\mu_J = g_J \mu_B J$$

where

$$\mu_B = \frac{e\hbar}{2m_e}$$

is the Bohr Magneton and g_J is the Land´e g-factor. similar argument goes for nuclear magnetic moment:

$$\mu_I = g_I \mu_B I$$

where

$$\mu_N = \frac{e\hbar}{2m_p}$$

is defined as Nuclear Magneton. Note that m_p and m_e are respectively the mass of proton and the mass of electron.

C. Magnetic Field due to Helmholtz Coils

In this experiment we will use Helmholtz coils.Helmholtz coils consists of two identical circular coils of wire, placed parallel to each other with their centers aligned. The coils are separated by a distance equal to their radius, and they are connected in series so that the current flows in the same direction through both coils. When a current is passed through the coils, a uniform magnetic field is produced in the region between the coils, with the direction of the field parallel to the axis of the coils. Helmholtz coils are often used in experimental physics and engineering applications to create a known and uniform magnetic field for various purposes. The equation of Helmholtz coils is:

$$B_{coils} = \frac{(0.9 \times 10^{-2}\text{Ni})}{a}(\frac{Gm}{A}) \tag{1}$$

Where coils have radius a, number of turns of N. Note that the current i is going through the wires. With our equipment we have determined that:
$N = 135$ turns
$a = 0.275$ m

D. The Breit-Rabi Formula

The energy eigenvalues determined from the hyper-fine structure Hamiltonian H_{Hfs} can also be calculated in the presence of a non-zero external magnetic field using the Breit-Rabi formula. In the electronic ground state of alkali atoms, the hyper-fine energy levels are split due to the interaction between the nuclear magnetic moment and the electron's magnetic moment. When a magnetic field is present, the energy levels are further split into Zeeman levels, with slightly different energies depending on the strength and direction of the magnetic field.

The Breit-Rabi formula describes the energy eigenvalues of these Zeeman levels in the presence of an external magnetic field. It takes into account the hyper-fine coupling between the nuclear spin and the electron spin, as well as the Zeeman effect due to the external magnetic field. The useful, simplified version of formula for our analysis is given by:

$$\frac{\nu}{B_{ext}} = \frac{2.799}{2I+1}(\frac{\text{MHz}}{\text{G}}) \tag{2}$$

Note that:

$$B_{ext} = B_{coil} + B_{amb} \tag{3}$$

where B_{coil} is the uniform magnetic field due to the coils and the B_{amb} is the ambient magnetic field. The source of this field is mostly due to earth's magnetic field plus the magnetic field due to the current in the wires of the other electricity powered tools in our lab.

E. Optical Pumping and ODMR

The precise determination of energy levels in atomic, molecular, nuclear, and particle systems represents a significant aspect of experimental physics. Optical pumping has emerged as a powerful technique for measuring the difference between atomic energy levels with extraordinary accuracy. In this study, we employ optical pumping to measure the splitting of rubidium atomic energy levels in the presence of a magnetic field.

The fundamental principle of optical pumping is based on the interaction of light with atoms. When an atom is subjected to light of a resonant frequency, it can absorb the energy of the light and transition to a higher energy level. Optical pumping generates spin polarization and represents a method for achieving such polarization. In this experiment, pumping occurs by exposing the atoms to infrared light that covers all transitions on the D1 line and has circular polarization.

In the m_f state, spontaneous emission induces a transition of the electron to the ground state, accompanied by a change in m_f of either +1, 0, or -1. Repeated occurrences of this process lead to the majority of atoms reaching the "maximally pumped" state. In Rb87, this state is characterized by F=2 and m_f=2 (for a magnetic field oriented in the +z direction), and F=2 and m_f=-2 (for a magnetic field oriented in the -z direction). In the case of Rb85, the maximally pumped state is identified by F=3 and m_f=3 (for a magnetic field oriented in the +z direction), and F=3 and m_f=-3 (for a magnetic field oriented in the -z direction). Note that this pumped state is regarded as a "dark state," as it no longer interacts with light. Or better said, at this state, the gas is no longer transparent to the emitted frequency, and it no longer absorbs the frequency but transmit it.

The utilization of the dark state, resulting from the process of optical pumping, presents the opportunity to detect radio frequency magnetic transitions within atomic vapor by optical means. This technique is commonly referred to as "optically detected magnetic resonance" (ODMR). The concept is straightforward: when the atoms are not stimulated by a resonant radio-frequency magnetic field, they are optically pumped into

a dark state, which no longer absorbs optical pumping light. A photodetector, measuring the light that passes through the atomic vapor, will register a high level of light.

III. METHODS AND PROCEDURES

In this section the procedures and methods and experimental setups are outlined.

A. Tools, equipments and Block Diagram

The experiment uses a spherical glass bulb coated with a thin wax layer, containing a low-density neutral buffer gas, and a small amount of rubidium. The rubidium is released into the buffer gas by heating the bulb, and its density is controlled by varying the temperature. A resistive heater is used for temperature control, and its interference with ODMR measurements is eliminated by switching it off during precise measurements. Rubidium atoms diffuse within the cell for a long time before striking the walls, allowing them to absorb and re-emit many optical pumping photons. Collision with the buffer gas conserves atomic spin, leading to the long lifetime of atoms in the pumped state. This setup enables precise optical detection of radio frequency magnetic resonance within the atomic vapor, by exploiting the property of the pumped state being a dark state. The experiment utilizes an optical pumping technique to measure the energy levels of rubidium atoms in a gas mixture. The optical pumping light is generated by a lamp containing rubidium gas in an electronic discharge. The light passes through two optical elements: a circularly polarizing optical polarizer and a D1 pass filter that allows light near 795 nm to pass through. The filtered light drives all D1 transitions within the addressed vapor cell, but not D2 transitions. The lamp's emission then shines upon a photodiode, which detects the light transmitted through the atomic vapor cell.

The atomic vapor is positioned between two nearby electromagnet coils, which are connected in series and are driven by a function generator. The current in this photodiode is amplified using an amplifier. A sinusoidal current is generated by the addressed function generator and sent through small rf coils that surround the Rb lamp. This produces a radio-frequency magnetic field that is perpendicular to both the optical axis and the axis of a strong external magnetic field, which is generated by the Helmholtz coils. Note that The vapor cell, heater, optical setup, and rf coils are all located within a light-proof, thermally insulating box. And again let us not forget coaxial, circular coils placed outside the light-proof box. These two coils are in the Helmholtz configuration (same radius and separation), and will provide a uniform magnetic field in the desired direction. The Helmholtz coils are powered by a current source that consists of a DC current, generated by a supply and an AC current. The AC current is produced by reducing the peak-to-peak voltage of the 60 Hz AC. This creates a magnetic field with both DC and AC components. The same AC voltage, with variable phase shift, is sent to the oscilloscope that monitors the photodiode signal. The Zeeman resonance frequency of the atomic vapor is regulated by the DC current, while the AC current modulation offers a precise and reliable means of identifying the magnetic resonance condition. All the described pieces of equipment could be seen on the fig.3 where the block diagram is outlined.

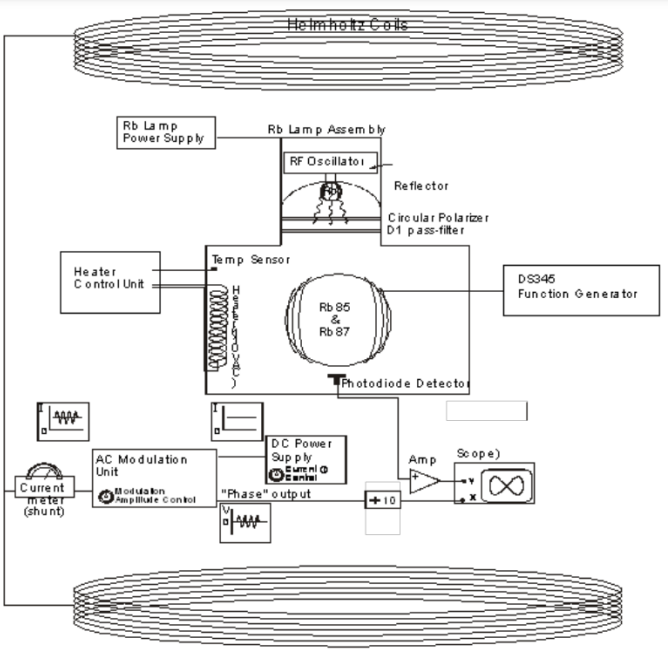

FIG. 3. A schematic of all the parts and circuitry of this experiment [1]

B. Procedures for Observation of ODMR

We started by turning on all the pieces of equipment. DC, AC function generator, heater, current meter, and oscilloscope, We were wary of the two important limits. First the current must not exceed 3 A and second, the heater's temperature must not exceed 55 C. An optimal setting for the preamp that we used was: Input 'A', with the DC/GND/Ac button on the AC position, gain initially to 500, the LF Roll-off to 0.1 Hz, and the HF Roll-off to 10 kHz, with both filters set at 6 dB per octave. We started with a temperature of 48 C. We also started with a DC current of 1 A through the Helmholtz coils.

We set the function generator to produce a sinusoidal current whose frequency was swept linearly, (and this is important.) with a 100 ms sweep period, over a 3 MHz

range The output voltage was initially set to 5 V peak-to-peak. Although at the end of the day, we set our start frequency to 1.7MHz and the stop at 3.6MHz.

We used the oscilloscope to measure the amplified photodiode signal vs. the frequency of the rf magnetic field in our experiment. The XY mode is employed for this purpose. We placed the "Modulation Output" of the function generator on the "X" axis (Channel 1). On the Y-axis (Channel 2), the photodiode signal was placed This signal comes right from the preamp. It is a good idea to turn off the heater to avoid the resonance jumping in the scope. The jumps happen because an unwanted magnetic field gets generated once the heater is on around the heater's wire. This magnetic field causes all the jumps on the scope screen. So once we wanted to focus for measure something we turned off the magnetic field. Now on the screen, we found the best sweep rate and centered the figure. The ODMR appeared. You can see the processed image we took from the scope's screen (processed for the sake of visibility). There the two resonance points are clearly visible. One of them corresponds to RB87 and the other to Rb85. Based on the start and stop point of the signal on the scope, we were able to make a ballpark estimate of these 2 frequencies. These estimates became critically useful and handy in our future procedures for finding the resonance points (refer to fig.4).

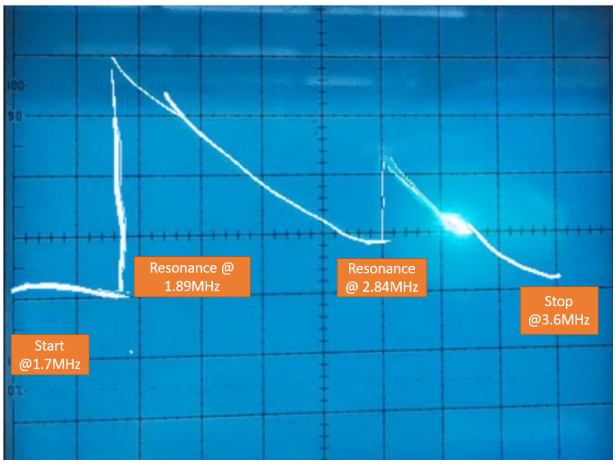

FIG. 4. Observation of ODMR. We have processed the photo taken from the screen to demonstrate this feature. Note that the stop, start, and the estimated values of the two resonance frequencies were all marked on the picture.

C. Optimal Bulb Temperature

With the ODMR signal of the two isotopes in view on the oscilloscope, we increased the temperature of the light-proof box to approximately 55 ∘C. The heaters were subsequently turned off. Over time, the temperature of the light-proof box decreased slowly. During this process, we took measurements of the height of the ODMR signals (in units of divisions; note that this part is only qualitative) for each isotope as a function of the box temperature (fig.5). With this method, we are able to determine the optimal temperature for our gas setup. The graph of the division vs. temperature is plotted and here we can see that the best visibility on the screen happens at around the temperature of 46 C. So from this point, we maintained the temperature of the heater close to this optimal temperature.

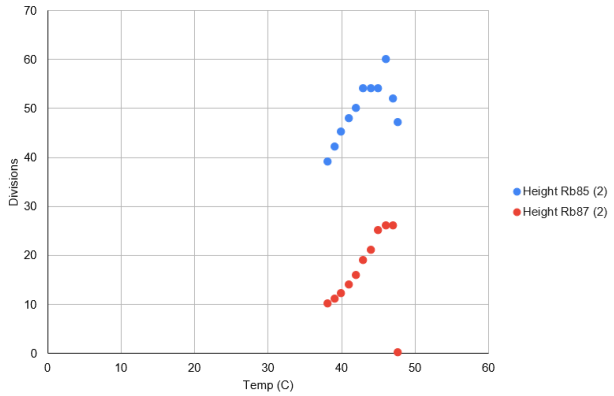

FIG. 5. The plot of scope's screen division vs. temperature for both isotopes. As suggested by the plot optimal temperature is around 46 C.

D. Current Modulation/Lock-in Detection of the Resonance Frequency

This part is the heart of our experiment! Now it is time to find the Zeeman resonance frequencies. the lock-in method detects an AC signal rather than a DC signal.we modulated (vary sinusoidally) the external magnetic field in order to make the detection of the signal more efficient and accurate. When the magnetic field is modulated, the resulting signal is an AC signal, which is easier to detect and measure compared to a DC signal. The lock-in amplifier is capable of detecting the signal at the modulation frequency while rejecting signals at other frequencies. This helps to eliminate noise from other sources that could interfere with our measurements. we selected 60 Hz as our modulation frequency

By modulating the current, we can rapidly, precisely, and accurately locate the center of the resonance response, we started by turning on the field modulation by flipping the "Field" switch on the Coil Driver panel and turning on the "Phase Out" output by flipping the "Phase Switch." The Phase Out signal tracks the 60 Hz modulation placed on the Helmholtz coils. This was our new channel 1 (X) of the scope. The photodiode voltage that is coming from the preamp is still our channel 2 (Y). The estimates of Zeeman frequencies that we got for the ODMR section proved to be very handy here. We used those estimates as a starting point for tuning into resonance frequencies for both Rb87 and Rb85.To find these

resonances with high accuracy and precision, we set the function generator to the estimated resonance frequency (with no frequency modulation), and then finely tuned the DC current around 1.0 A until the resonance is observed and then from that point, we started by taking the increments of 0.2 A above the 1.0A current. The clue that told us when we are at the resonance frequency is the appearance of the Lissajous figure (fig.6). Note that current is our independent variable. Once the current was changed it was time for frequency to change. And we changed the frequency finely until the Lissajous figure appears on the scope's screen. Sometimes it was needed to also play with the phase knob on the settings. This allows us to see the Lissajous figure from a different angle. Note that merely observing a Lissajous figure is not enough. The Lissajous must be symmetrical and a non-symmetrical Lissajous is not acceptable. A non-symmetrical Lissajous is simply suggesting that we are still not in resonance frequency and we still need to vary the frequency a bit more. Naturally, a perfect symmetric Lissajous means that we are indeed at the perfect resonance frequency. This process is repeated for each isotope. Once these measurements were all done, we reversed the current direction by switching the reverse key on the control interface to scan through the negative side of the current. We did the same data point acquisition but with negative current. At the end of the measurement, we had 4 data sets. 2 for Rb87 with two different current directions and 2 for Rb85 with two different current directions. For the sake of handling the uncertainty and error in our experiment, since the error is of the heteroscedastic type, we evaluated an upper and lower bound for each data point. The upper and lower bounds were determined in such a way that exceeding these limits results in the Lissajous' symmetry deformation. With this technique, we were able to identify an error margin for each data point in the Y-axis.

We also performed an extra measurement. It was the observation of the zero-field resonance. The observation of a zero-field resonance was carried out by turning off the rf modulation entirely and scanning the current. A resonance feature was found to exist even when the Helmholtz field precisely canceled the ambient field along the optical axis. The reason why we took this measurement and why there still exists a resonance point will be addressed in the analysis section.

E. Timescales for Optical Pumping Using Square Wave Amplitude Modulation of the rf Field

In order to get some estimate for 1/e time scale (optical pumping relaxation time), we Configured the rf-generator to produce a sinusoidal signal that is amplitude modulated by a square wave of low frequency, with the sinusoidal signal frequency set to match the rf resonance frequency. The amplified photodiode signal can then be monitored as a time trace on the oscilloscope. Note that

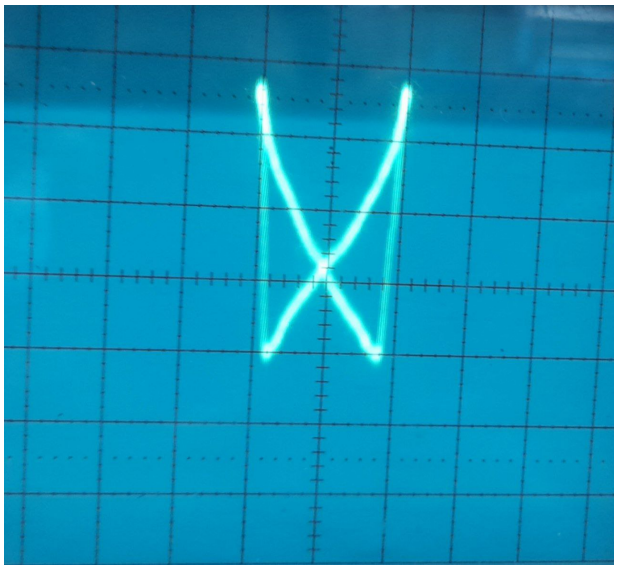

FIG. 6. The appearance of a symmetric Lissajous figure on the scope

we switched from our good old analog scopes to modern scopes, since measuring this time trace was not doable on the old scopes. Detailed analysis and comments on the obtained results will be provided in the analysis section.

IV. DATA ANALYSIS AND RESULTS

Here we are releasing the whole sets of data and performed analysis done on those previous outlined experiments. You can also find a more in depth discussion of the covered topics in methods and procedure section here as well.

A. Frequency vs. Current

Here we have the raw data plotted(fig.7). After multiplying the current and frequency of the "reversed current" samples, we get the second plot (fig.8). The trend is truly close to linear regression, so we have done a line fit using Scipy.curvefit function from Python various libraries. The degree of freedom here is two. The fit parameters are just a slope and a y-intercept. (fig.9) The fit is in fact a weighted fit. And the errors in taking the data points are already incorporated into the fit function. You can see the error margins for the Y-direction (Note that it is Y direction, we have not done the error in the X direction, because tracking down the error in Y is indeed more applicable and physical.) In this experiment, the errors on the data points tend to be too small to be visible when plotting them(as you could probably say so in fig.9) So because of that we have prepared the plot of the residuals. This is a plot that actually shows the amount of deviation of the data

point from the line of best fit (fig.10). There seems to be indeed good consistency in the errors. All in all The residuals seem to be fairly small, and in fact, the errors are really hard to distinguish on fig.9 so the residual plot does really help to get a feeling about the deviation of the data points from the fit line. Our reported value for slope and y-intercept for the weighted curve fitting (data point in data set as weights within the linear regression formulae) are as follows:

For Rb87:
Slope: (2.0340 ± 0.0016) MHz/A
Intercept: (-0.1972 ± 0.0018) MHz

For Rb85:
Slope: (3.0424 ± 0.0010) MHz/A
Intercept: (-0.3000 ± 0.0013) MHz

These two remarkable findings are the ones that we are going to use from now on. Since these are the error estimates derived for each data point as weights and already incorporated into the fitting procedure. But for the sake of completeness, we will include the error estimates derived for each data point unweighted. After the (unweighted error) fitting procedure we found that:

For Rb87:
Slope: (2.0293 ± 0.0010) MHz/A
Intercept: (-0.1972 ± 0.0015) MHz

For Rb85:
Slope: (3.0426 ± 0.0006) MHz/A
Intercept: (-0.3021 ± 0.0009) MHz

The use of appropriate error estimates is critical for data fitting and should be taken into account when performing linear regression. If these two methods lead to different fit results and error estimates, there could be several reasons why this might be the case. One possible reason is that the error estimates derived for each data point may not be accurate or may not reflect the true uncertainties in the measurements. Fortunately, in this case, our findings are closely consistent with each other. If the fit results and error estimates using the two methods of error estimation (weighted and unweighted) agree with one another, it suggests that the errors in the data set are well-characterized and that the linear regression model is a good fit for the data. This fact is well demonstrated by our data.

Now It is time to evaluate the goodness of our fit by other measures. The Chi-sqr method is a widely used statistical test that provides a quantitative measure of how well a model fits the observed data. This method involves comparing the observed data with the expected values based on the model and calculating a statistical critical value called the Chi-sqr value. The lower the value of Chi-sqr, the better the fit of the model to the

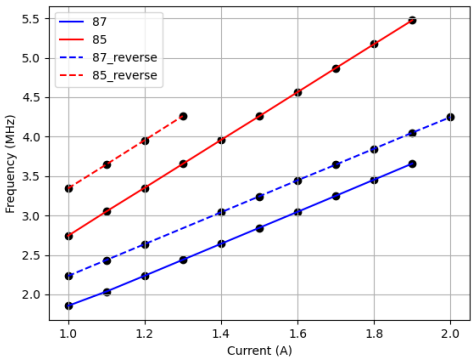

FIG. 7. A plot of the raw data points

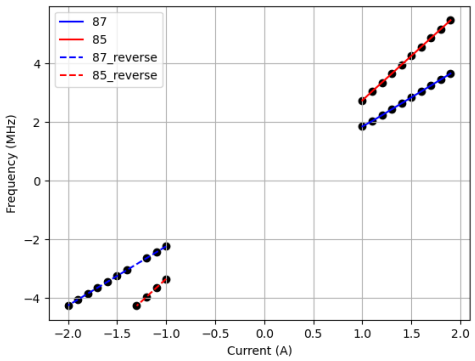

FIG. 8. Here it is shown that how the data processed to let us deal with 2 lines instead of 4 lines. This makes the whole analysis section a lot cleaner and easier to deal with. Note that the current and frequency of the "reverse magnetic field" got multiplied by a (-1). Also note that the missing data points were interpolated.

data. Here we used the this equation of the Reduced chi-square:

$$\chi^2 = \frac{\sum_{i=1}^{n} (\frac{observed_i - model_i}{error_i})^2}{n-2}$$

Where the number 2 comes into the equation because we only have 2 degrees of freedom in our linear regression. We proudly like to announce that our χ^2 values are:

$$\chi^2_{Rb87} = 1.21$$

$$\chi^2_{Rb85} = 5.92$$

The calculated value of the chi-sqr statistic for our data is remarkably low, and very close to 1. This suggests that the model used to fit the data is a fine representation of the observed values, and that the residuals are very small. This is a strong indication that the data is of high quality, and that the experimental methods used

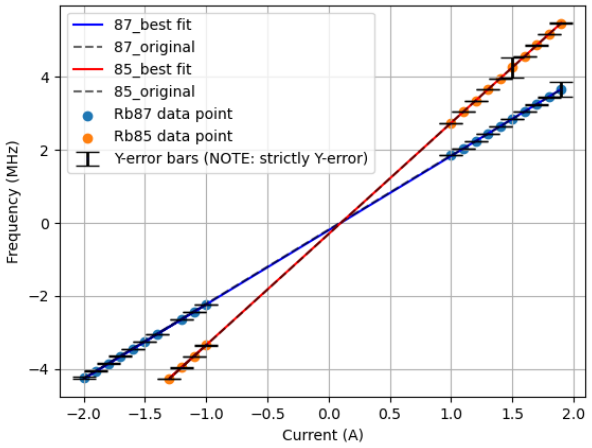

FIG. 9. The final plot of frequency vs. current for both isotopes with **Vertical** error margin bars.Note that the error bars are not a good indicator here. Since the error margin is very small, the error bars are technically not so expressive. So a better way to present the error bars is the residual plot (fig10)

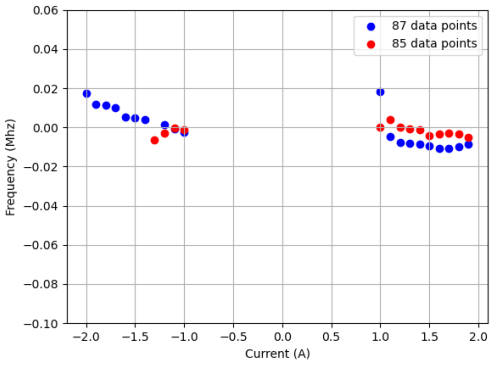

FIG. 10. The plot of the residuals. This is a better way to compare the errors. You can see the deviation of each data point from the actual best fit line

to obtain the data are accurate and reliable. The small value of chi-sqr also implies that the uncertainty in the measurements is well-characterized and that the model parameters have been estimated with a high degree of precision.

It is worth noting that our data acquisition could be also problematic at some points. Due to several reasons, we were unable to record the data between current = -1 and current = 1. Hence there is a data point gap in this region. If we were able to get back in time, we would have made this correction and covered that gap with a good amount of data points. But right now the best we could have done was (as you can see) to interpolate in between the missing data points and then do the linear regression on the final observational model. We believe that this inconsistency will introduce an underestimate in error and uncertainty. And this to an extent makes sense, considering our very excellent chi-sqr value. Nevertheless, this experiment is quite rewarding so far and the data is serving us well.

B. The Ambient Field

One of our goals in this lab is to measure the ambient field. As outlined the external magnetic field consists of the coils' magnetic field plus the ambient field. The ambient field is not necessarily the earth's magnetic field, but rather than that could be the artificial field generated by the currents in the wires as well. We will present two methods to calculate this field. The first method is a quick but rather imprecise way to do so. This approach for determining the ambient magnetic field is to make a preliminary estimate by measuring the current at which the magnetic field generated by the coils is effectively canceled out. This is accomplished by searching for the current value at which the oscilloscope displays a relatively flat response with minimal resonance, indicating that the ambient field has been successfully neutralized. We measured this current to be at 0.0941 A. By plugging in this into equation1 we can report that the calculated ambient field value is $B_{amb} = 0.415G$. It was challenging to report the uncertainties with this method.

The other method of finding the ambient field is way more systematic and general. It is also the basis of finding the "I" quantum numbers in the next subsection. We have a bit of theoretical analysis to start. We start with equation**??** the Breit-Rabi formula:

$$\frac{\nu}{B_{ext}} = \frac{C}{2I+1}(\frac{\text{MHz}}{\text{G}})$$

Where C is just the constant 2.799.
Now since the $B_{ext} = B_i + B_{amb}$ (the external magnetic field is ambient field plus the field due to Helmholtz coils) we have

$$\frac{\nu}{B_i + B_{amb}} = \frac{C}{2I+1}(\frac{\text{MHz}}{\text{G}})$$

Now according to equation1 we can rewrite B_i:

$$\frac{\nu}{Ki + B_{amb}} = \frac{C}{2I+1}(\frac{\text{MHz}}{\text{G}})$$

Where

$$K \equiv \frac{0.9 * 10^{-2} N}{a}$$

Now by rearranging the above equation we have:

$$\nu = (\frac{CK}{2I+1})i + (\frac{C}{2I+1})B_{amb}$$

So we can clearly see that in a frequency Vs. current linear plot:

$$Slope = \frac{CK}{2I+1} \tag{4}$$

$$y - int = (\frac{C}{2I+1})B_{amb} = (\frac{slope}{K})B_{amb} \qquad (5)$$

This is a very powerful way to find the ambient field. So according to equation5 we can conclude that the ambient magnetic field is:

Ambient field for Rb87 = (-0.4282 ± 0.004)G
Ambient field for Rb85 = (-0.4352 ± 0.006)G

Note that the negative sign just refers to the direction and polarity of the field. These values match quite well with our first approach. And note that 0.4G fall easily in the accepted range for the value of the earth's magnetic field which is between 0.25G and 0.65G (There is no way to establish a single number as earth's magnetic field as it varies a lot depending on the location.)! This is yet another success in our measurements, calculations and results!

C. Calculation of Nuclear Spin

By using and leveraging most of the work in the previous subsection, we can find the value of the nuclear spin I for each individual isotope. The relationship derived equation 4 allows for the determination of I_{85} and I_{87} individually through linear fits to the respective data sets. So after the calculations, we obtained that:

$$I_{85} = 2.539 \pm 0.004$$

$$I_{87} = 1.532 \pm 0.006$$

Which to no surprise they resemble the numbers 5/2 and 3/2. The percent difference for the perfect ratios are 2.1% and 1.7% for Rb87 and Rb85 respectively. This is indeed a good accomplishment. The errors are all trace back to slopes and y-int and even these trace back further to the uncertainty in our data points.

There is another method to evaluate these nuclear spin numbers.Which is more of an analytical approach. To determine the nuclear spins of Rb85 and Rb87 isotopes, we should start by taking the ratio of their Zeeman resonance frequencies ν_{85}/ν_{87} and using the Breit-Rabi formula to calculate the spins "by hand". This process requires rearranging the Breit-Rabi equation and the magnetic field equation of the Helmholtz coils (as a function of current) to determine the relationship between the resonance frequency and the nuclear spin quantum number for each isotope. To determine the best ratio of ν_{85}/ν_{87}, the overall data set is analyzed through fits while considering sources of error retained or eliminated by the analysis method. With the ratio determined, the values of I85 and I87 can be deduced, which should be exactly half-integral. It is also possible to use the ratios of the magnetic fields acquired in the previous subsections. In any case we should end-up getting 5/2 and 3/2 analytically.

D. Time Scale for Optical Pumping and other Final Remarks and Miscellaneous topics

We were able to estimate the "pumping time" (1/e) for the non-pumped gas to become optically pumped. the time scale for optical pumping depends on several factors and can vary widely depending on the specific system and experimental conditions. For the RB85 (we could not do the same for RB87 because the scope got too laggy and fuzzy) we happened to see a damped oscillation. This is because of many reasons such as spin relaxation in collisions, spin relaxation upon striking the wall of the glass cell, magnetic field inhomogeneity, and light scattering. Our rough estimate for the relaxation time (1/e) is around 64 ms, and for the pumping time, it was around 100 ms (half of the square-wave wavelength).

The other remark is about the existence of resonance at zero field. A potential explanation for this phenomenon that we came up with is that In the context of magnetic resonance, the resonance condition is achieved when the energy difference between two energy levels matches the energy of the electromagnetic radiation applied to the sample. At zero field, the energy levels are degenerate and therefore have the same energy, so the resonance condition can be satisfied by applying electromagnetic radiation with a frequency that matches the energy difference between the degenerate levels. And once again we can observe those symmetric Lissajous figures. But note that it is not easy to tune into this frequency.

Lastly, it is worth mentioning that since we know all about the current i and the frequency, and the nuclear spin I, we can easily deduce the magnetic field using the Breit-Rabi equation (equation2). So knowing the current is equivalent to knowing the magnetic field.

V. CONCLUSION

To conclude, in this report, the phenomenon of optical pumping was demonstrated, where atoms were excited from a lower energy state to a higher energy state through the absorption of light of a specific frequency. Through careful data analysis, the ambient magnetic field was determined. these values were found to be consistent with the expected range for the Earth's magnetic field, demonstrating the accuracy of the experimental measurements. In addition, the nuclear spin number of the Rb85 and Rb87 isotopes was determined using the linear relationship between the resonance frequency and the magnetic field strength (current). The obtained values were found to be in excellent agreement with the expected values of 5/2 and 3/2. And finally, an in-depth error analysis was performed on the results.

VI. REFERENCES

OPT - OPTICAL PUMPING Physics 111B: Advanced Experimentation Laboratory University of California, Berkeley [1]

OPTICAL PUMPING OF RUBIDIUM VAPOR University of Princeton [2]

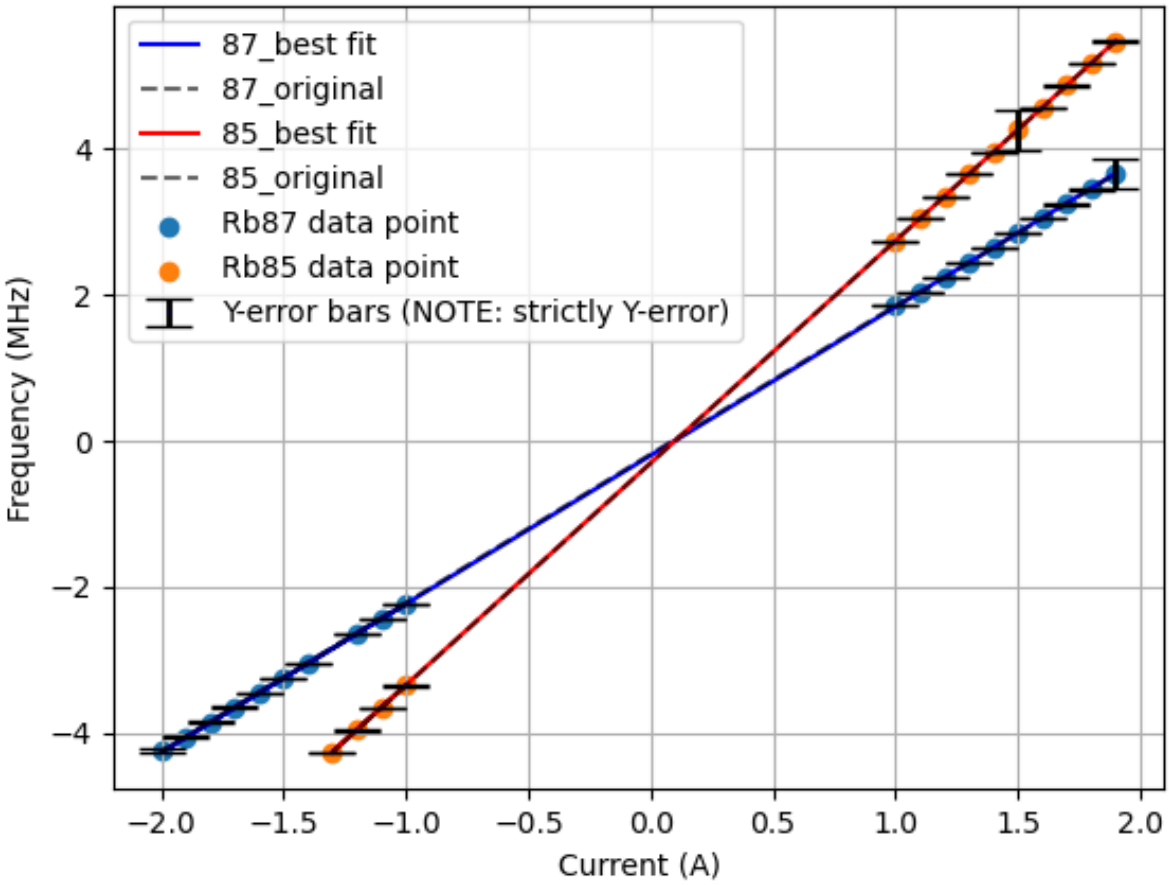

FIG. 11. For the sake of the importance of the plot, an enlarged version of the fig.9 is placed here

up	Rb87				Rb85		
	freq (MHz)	lower MHz	upper MHz	current	freq(MHz)	lower	upper
1	1.855	1.8538	1.8544	1	2.7427	2.7423	2.7436
1.1	2.0357	2.0353	2.0368	1.1	3.0509	3.05	3.0516
1.2	2.2361	2.2357	2.2367	1.2	3.3509	3.3502	3.3514
1.3	2.4388	24384	2.4395	1.3	3.6544	3.6537	3.6551
1.4	2.6419	2.4616	2.643	1.4	3.9583	3.957	3.9592
1.5	2.8444	2.8438	2.8452	1.5	4.2593	4.2583	4.2603
1.6	3.0466	3.0456	3.0474	1.6	4.5644	4.5627	4.5653
1.7	3.2499	3.2491	3.2513	1.7	4.8694	4.8681	4.871
1.8	3.4543	3.4531	3.4554	1.8	5.173	5.1702	5.1754
1.9	3.6589	3.6578	3.66	1.9	5.4754	5.4724	5.4774
2	3.865	3.8634	3.8662	2	5.7804	5.7784	5.7844

polarity down	Rb87			Rb85			
current	freq (MHz)	lower (MHz)	Upper (MHz)	current	freq (MHz)	lower (MHz)	Upper (MHz)
1	2.2336	2.2331	2.2346	1	3.3435	3.343	3.346
1.1	2.4354	2.4351	2.4361	1.1	3.647	3.646	3.649
1.2	2.6368	2.6361	2.6383	1.2	3.954	3.95	3.957
1.4	3.041	3.0368	3.044	1.3	4.2617	4.2579	4.2641
1.5	3.2434	3.2395	3.2446				
1.6	3.4464	3.4434	3.4494				
1.7	3.645	3.645	3.652				
1.8	3.847	3.84	3.852				
1.9	4.05	4.038	4.052				
2	4.248	4.234	4.263				

FIG. 12. For reference a table of acquired raw data is included here